Observation of pseudo-two-dimensional electron transport in the rock salt-type topological semimetal LaBi

Nitesh Kumar,[1] Chandra Shekhar,[1,*] Shu-Chun Wu,[1] Inge Leermakers,[2] Olga Young,[2]
Uli Zeitler,[2] Binghai Yan,[1] and Claudia Felser[1,†]

[1]*Max Planck Institute for Chemical Physics of Solids, 01187 Dresden, Germany*
[2]*High Field Magnet Laboratory (HFML-EMFL), Radboud University, Toernooiveld 7, 6525 ED Nijmegen, The Netherlands*

Topological insulators are characterized by an inverted band structure in the bulk and metallic surface states on the surface. In LaBi, a semimetal with a band inversion equivalent to a topological insulator, we observe surface-state-like behavior in the magnetoresistance. The electrons responsible for this pseudo-two-dimensional transport, however, originate from the bulk states rather topological surface states, which is witnessed by the angle-dependent quantum oscillations of the magnetoresistance and *ab initio* calculations. As a consequence, the magnetoresistance exhibits strong anisotropy with large amplitude ($\sim 10^5$%).

Topological insulators (TIs) are characterized by their conducting surface states due to the nontrivial topology of the bulk band structure [1,2]. A three-dimensional (3D) topological insulator has topologically protected conducting surface states in the form of an odd number of Dirac cones. Not limited to insulators, topological states have also been observed in semimetals, for example, Weyl semimetals and Dirac semimetals in which conduction and valence bands disperse linearly through nodal points in all directions in the three-dimensional space [3–7]. When these bands are doubly degenerate, the system is called a Dirac semimetal. If the degeneracy is lifted by breaking time reversal and/or inversion symmetry, properties of a Weyl semimetal can be observed. Weyl semimetals exhibit exotic Fermi arcs in the surface states [3] and interesting transport phenomena, such as extremely large magnetoresistance (MR) and high charge-carrier mobility [8,9]. A group of topological materials exists, however, with a zero energy gap, which is actually semimetallic and referred as topological semimetals (TSMs). For example, the Heusler TIs usually exhibit an inverted band structure and the gapless feature at the Fermi energy [10–12]. Large MR and high mobility were also reported in these compounds, such as LaPtBi [13,14]. However, it is still illusive to distinguish the contributions by the bulk and surface states to the transport properties because of the semimetallic nature of TSMs.

Recently, a new series of compounds, lanthanum monopnictides, was theoretically predicted to be TSMs [15], which stimulates the interest in their transport properties [16]. The last member LaBi is particularly interesting because of the largest spin-orbit coupling, which may result in topological surface states. Observation of several Dirac cones in LaBi by angle-resolved photoelectron spectroscopy has further increased the interest in this material [17]. Our experiments reveal a large unsaturated MR in LaBi, which is due to the electron-hole compensation in this semimetallic material. We observe a remarkable transverse MR on the order of

10^5% along with strong anisotropy which brings it in the line of the best-known materials, such as NbP, WTe$_2$, and NbSb$_2$ [8,18,19]. Strong Shubnikov–de Haas (SdH) quantum oscillations develop at low temperatures, which enable us to reconstruct the Fermi-surface topology. The Fermi-surface topology extracted from angular-dependent magnetotransport experiments agrees well with our *ab initio* calculations. We observe an interesting strongly anisotropic Fermi surface that originates from the bulk electron pockets rather than real surface states.

High-purity La and Bi metals were weighed and transferred into an alumina crucible according to the composition La$_{0.33}$Bi$_{0.67}$ (15 g) inside an argon-filled glove box. The crucible was sealed in a quartz vessel under 3-mbar Ar pressure to avoid the La attack on the quartz tube. The contents were heated at 1250°C with a heating rate of 100°C/h. This temperature was maintained for 1 h followed by cooling to 1200°C with a rate of 100°C/h. After this the content was slowly cooled (1°C/h) until 1050°C for crystal growth. At this temperature the extra Bi flux was decanted out, and the content was rapidly cooled down to room temperature. Cubic crystals of LaBi were retrieved and stored inside a glove box. The quality of the crystals was checked by using a single-crystal x-ray diffraction Bruker D8 VENTURE x-ray diffractometer with $Mo - K\alpha$ radiation and a bent graphite monochromator.

The transport measurements were performed using the ac transport measurement system rotator option of the physical property measurement system (Quantum Design) with a maximum field of 9 T. The 35-T static magnetic-field measurements were performed at the High Field Magnet Laboratory HFML-RU/FOM, a member of the European Magnetic Field Laboratore in Nijmegen. Linear electrical contacts were made by 25-μm Pt or 40-μm Au wires using Ag epoxy as glue.

The Vienna *ab initio* simulation package was adopted to perform the density-functional theory calculations [20,21]. The hybrid functional (HSE06) [22] with spin-orbital coupling was used to calculate the electronic structures. The bulk Fermi surfaces and the band structures were interpolated by maximally localized Wannier functions [23–25]. The experimental lattice constant $a = 6.5797$ Å of rock salt LaBi was adopted.

*Corresponding author: shekhar@cpfs.mpg.de
†Corresponding author: felser@cpfs.mpg.de

LaBi has the largest spin-orbit coupling of all lanthanum monopnictides, and it readily grows with Bi as a self-flux in contrast to, e.g., LaSb where tin is used as the flux and creates a possibility for elementary tin inclusion in the crystals. Moreover, LaBi is more stable than LaSb in air and moisture. It crystallizes in the rock salt structure with space group Fm-$3m$ wherein La and Bi atoms are arranged alternatively in all three directions. The crystals obtained from Bi-flux growth are well-faceted cube shaped with smooth (100) faces and can easily be cleaved along these faces.

We measured the electrical transport of our well-oriented crystals (as confirmed from Laue diffraction) at temperatures down to 350 mK and magnetic fields up to 35 T. The current was applied along [100], and the field was rotated along different directions of the crystals. In order to improve statistical significance we have reproduced the measurements on many crystals. At zero magnetic field, the resistivity ρ shows purely metallic behavior and decreases linearly with temperature until 65 K below which it shows Fermi-liquid behavior with $\rho_0 + aT^2$ relation (see Supplemental Material Fig. S1 [26]). The resistivity values are $4.95 \times 10^{-5}\,\Omega$ cm at 300 K and $1.46 \times 10^{-7}\,\Omega$ cm at 2 K resulting in a residual resistivity ratio $(r_R) = 339$ confirming the high crystal quality, in fact, the residual resistivity of LaBi is even less than in other known semimetals (WTe$_2$, NbP). Moreover, the conductivity per unit charge carrier at 300 K is on the same order as in highly metallic elements, such as copper.

When a magnetic field is applied, a metal to insulator like transition is observed at low temperatures, and the transition temperature increases with increasing magnetic field [Fig. 1(d)]. This was first observed in graphite, but now it is well known for many semimetals possessing high mobility [8,18,19,27,28]. This phenomenon has broadly been attributed to the formation of excitons resulting in opening

up of an excitonic gap in the material, which is enhanced in the magnetic field [27]. Semimetals with a smaller carrier density resulting in ineffective Coulomb screening and high mobility are ideal candidates to show metal to insulatorlike transition. This behavior can also be understood by scaling the temperature-dependent resistivity curves at different fields according to Kohler's rule as observed in WTe$_2$ [29]. This behavior is illustrated by plotting the MR versus $\mu_0 H/\rho_0$ for different temperatures (Fig. S2 in the Supplemental Material [26]). They all merge into the single behavior, which fits to the equation,

$$\mathrm{MR} = A(\mu_0 H/\rho_0)^m,$$

where A is a proportionality constant and m is the exponent. From the best fitting, $m = 1.6$($m = 2$ corresponds to the perfectly compensated electron and hole system), which points out the compensated nature of LaBi. Moreover, the normalized temperature-dependent MR values at different fields fall on top of each other. Hence, the low-temperature phase is a metallic phase rather than an insulating one in a high magnetic field. Transport at low temperatures is dominated by electron charge carriers with a crossover temperature between 10 and 20 K (see Supplemental Material Fig. S8 [26]) after which the hole charge carriers dominate.

Now we focus on the MR of LaBi, defined as MR(%) = $100 \times [\rho(B) - \rho(0)]/\rho(0)$. This material exhibits a huge transverse MR at 2 K and 9T [0.82×10^5%, see Fig. 2(b)] when the magnetic field is applied along [001]. Another crystal with lower $r_R = 193$ exhibited smaller magnetoresistance (0.38×10^5%) under the same conditions. The MR of both crystals increases quadratically with field. Extending the magnetoresistance measurements of LaBi to 35 T, we do not observe any sign of saturation (see Supplemental Material Fig. S9 [26]). The unsaturation behavior at high magnetic field
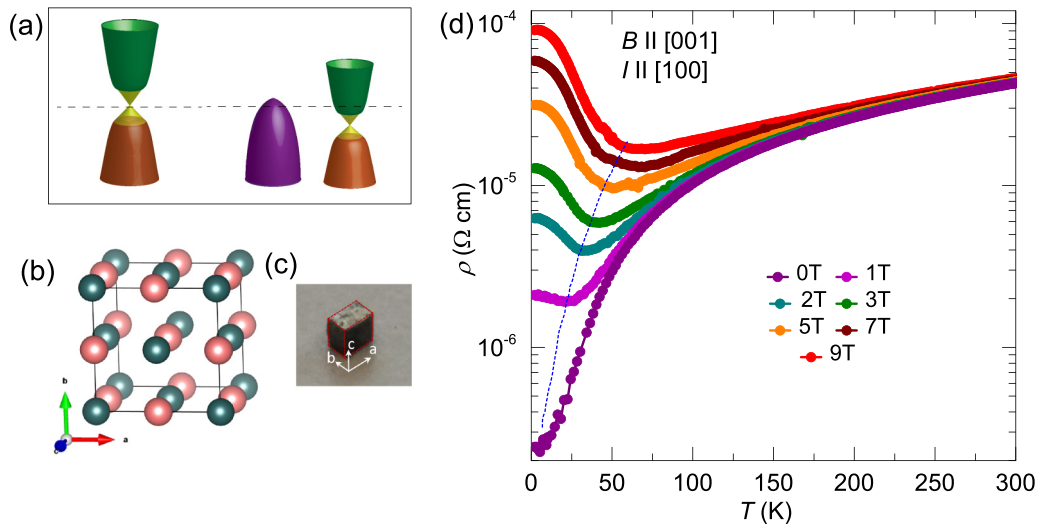

FIG. 1. Schematic band structure, unit cell, photograph of the crystal, and temperature-dependent resistivity of LaBi. (a) Schematic band structure of an ideal topological insulator (left panel) where the topological gap and the corresponding surface states are at the Fermi energy. Schematic band structure of LaBi with the topological gap and the surface states below the Fermi energy (right panel) in addition to a trivial valence band crossing the Fermi energy. (b) Crystal structure of LaBi where La and Bi are represented with red and green spheres, respectively. (c) Typical crystal of LaBi obtained from the flux growth technique where crystal edges are marked with red dashed lines. (d) Temperature-dependent electrical resistivity of LaBi at 0 T and fields up to 9 T. The blue dashed line is a guide to the eye to track the metal to the insulator like transition with increasing field.
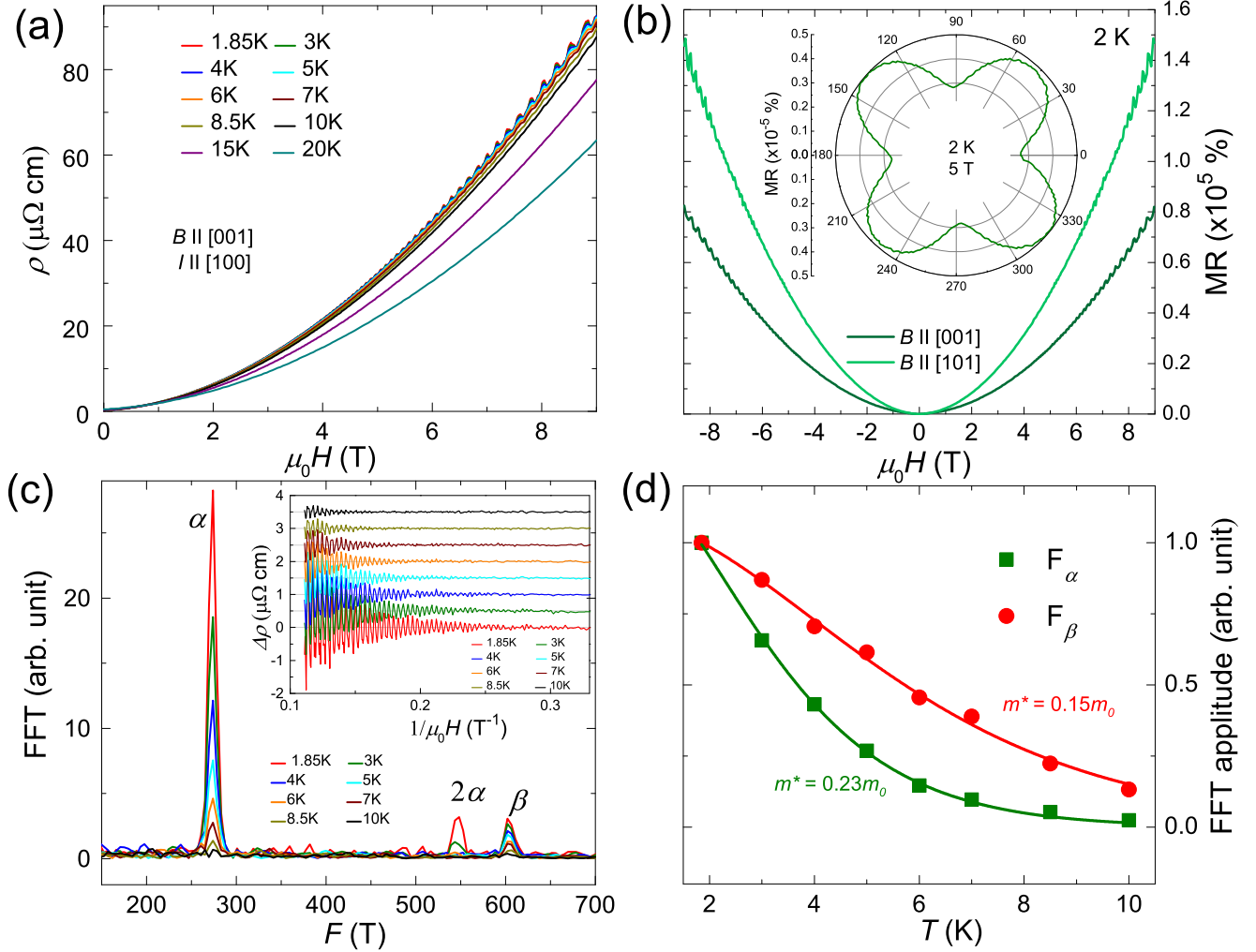
FIG. 2. Magnetoresistance and SdH quantum oscillations of LaBi. (a) Field-dependent transverse resistance of LaBi at different temperatures starting from 1.85 to 20 K with a maximum field of 9 T. (b) Transverse magnetoresistance of LaBi at fields along [001] and [101] directions at 2 K. The inset of (b) shows the polar plot of MR at 5 T wherein maxima and minima occur at fields along the [101] and [001] family of directions correspondingly. The inset of (c) shows SdH quantum oscillations after subtraction of a third-order polynomial plotted against the inverse of the magnetic field at temperatures from 1.85 to 10 K. (c) Corresponding FFT amplitudes of SdH oscillations depicting fundamental frequencies F_α (274 T), F_β (603 T), and the second harmonic of F_α (546 T). (d) Temperature-dependent FFT amplitudes of F_α (274 T) and F_β (603 T) along with their fittings according to Lifshitz-Kosevich relation to obtain their corresponding effective masses.

has only been demonstrated in very few materials, such as NbP and WTe$_2$. The value of MR does not change significantly until 15 K after which it decreases sharply. Interestingly, we observe 100% of further enhancement in the MR when the field is along [101] (MR = 1.5×10^5 %, 2 K and 9 T) compared to [001] (MR = 0.8×10^5 %, 2 K and 9 T) field direction. This anisotropic behavior in the MR is visualized in the polar plot of the resistivity where maxima and minima occur along [101] and [001], respectively [the inset of Fig. 2(b)]. Such a large MR anisotropy in LaBi is a clear indication of anisotropic Fermi-surface character. In contrast, LaSb shows only a 30% increase in MR along the [101] direction indicating smaller anisotropy compared to LaBi. *Ab initio* calculations [30] clearly show the larger anisotropy in LaBi compared to LaSb, which will be discussed further in the following sections.

The field-dependent resistivity shows SdH quantum oscillations, which are detected at low temperatures and fields as

low as 2 T. To extract their amplitude of the oscillations, a third-order polynomial was subtracted from the resistivity; the resulting oscillations at different temperatures are plotted against the inverse magnetic field [the inset of Fig. 2(c)]. These oscillations are highly periodic, and their amplitudes diminish with increasing temperature beyond 10 K. We employed a fast Fourier transform (FFT) in order to extract the frequencies involved in the oscillations [Fig. 2(c)]. We notice that two fundamental frequencies, F_α at 274 T from the electron pocket, α and F_β at 603 T from the hole pocket, β, as well as the second harmonic of the α pocket at 547 T are observed when B is along [001]. The temperature dependence of the FFT amplitudes of the corresponding Fermi pockets is shown in Fig. 2(d), which follow the Lifshitz-Kosevich relation,

$$\frac{\Delta\rho_{xx}}{\rho_0} \propto e^{-2\pi^2 k_B T_D/\beta} \frac{2\pi^2 k_B T/\beta}{\sinh(2\pi^2 k_B T/\beta)},$$
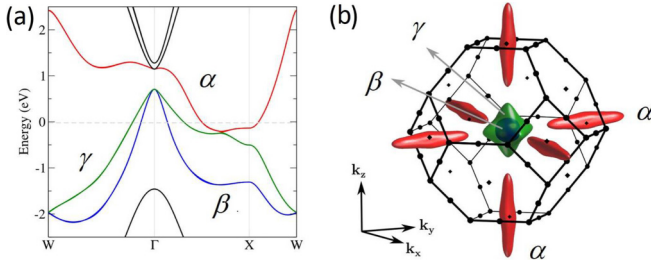
FIG. 3. Band structure and the first Brillouin zone of LaBi. (a) Bulk band structure of LaBi. The gray dashed line is the Fermi energy 20 meV below the compensation point. A topological gap appears near the X point of the Brillouin zone. (b) The Fermi surface in the first Brillouin zone at the Fermi energy. There are two hole pockets centered at the Γ point (β and γ) and three identical electron pockets (α) centered at the X points.

where k_B is Boltzmann's constant and T_D (Dingle temperature) and $\beta = ehB/2\pi m^*$ (with m^* being the effective mass) are fitting parameters. Best fitting yields the values for m^* and T_D of $0.23\,m_0$ and 8.9 K for the α pocket and $0.15\,m_0$ and 9.1 K for the β pocket, respectively, where m_0 is the bare electron mass. We analyze the most dominant frequency corresponding to the α pocket to obtain various parameters related to the Fermi surface, which play a significant role in electrical transport. Considering the circular cross section of the Fermi surface along [001], the Fermi area (A_F) that is covered by electrons is found to be $0.026\,\text{Å}^{-2}$ from Onsager relation $F = [h/(4e\pi^2)]A_F$ where F is the frequency of oscillation. A_F is used further to obtain the Fermi vector $k_F = 9.1 \times 10^{-2}\,\text{Å}^{-1}$. According to the relations $m^* = E_F/v_F^2$ and $v_F = \hbar k_F/m^*$ the values of the Fermi energy (E_F) and the Fermi velocity (v_F) are 2.76 meV and 4.6×10^4 m/s, respectively.

Our *ab initio* calculations clearly show the presence of electron and hole pockets located at the Fermi level. However, their presence can also be observed experimentally in a nonlinear Hall resistivity which otherwise should behave linearly. We observed a nonlinear Hall effect with a positive Hall constant at low fields, which changes its sign at higher fields. On increasing the temperature, the Hall constant is positive in the entire field range. In order to quantitatively determine the carrier densities we calculate the Hall conductivity tensor (σ_{xy}) and apply a two-band model to separate carrier densities and their corresponding mobilities. The resultant hole and electron densities are 7.56×10^{20} and 7.62×10^{20} cm^{-3}, respectively, and the corresponding mobility values are 1.89×10^4 and 1.75×10^4 cm^2 V^{-1}s^{-1}, respectively, at 2 K. This is in accordance to the compensated nature of LaBi. High carrier concentration and large mobility explain the excellent conductivity in LaBi compared to other semimetals. Fitting longitudinal conductivity tensor (σ_{xx}) also gives comparable values of carrier densities and mobilities validating the application of the two-band model (see Supplemental Material Fig. S8 [26]).

The band structure along high-symmetry lines for LaBi is shown in Fig. 3(a). The Fermi energy is 20 meV below the ideal electron-hole compensation point in the calculated band

structure and crosses three doubly degenerate bands (blue, green, and red). The blue and green bands are hole pockets, and the red bands are electron pockets. The band crossing points near X points between La-$5d$ and Bi-$6p$ states present the band inversion indicating a 3D topological insulator. The exact position of the Fermi energy $E_F(-20\,\text{meV})$ is determined by comparing the calculated angular dependence of the extremal cross-sectional area to the measured quantum oscillation frequencies. Calculations reveal two hole pockets (β and γ) and three electron pockets (α) in the first Brillouin zone. These electron pockets are identical in shape, and they are located at every X point. α and γ are strongly anisotropic as shown in Fig. 3(b), but the pocket β is nearly spherical and lies entirely inside γ at the Γ point. All pockets have only one extremal orbit when the field is applied along the crystallographic axes.

Experimentally, by tracking the angle-dependent SdH frequencies it is possible to reconstruct the entire Fermi surface. In this process, we rotate the whole resistivity setup to track how the SdH oscillation frequency F changes as a function of the tilt angle with respect to the field in a broad range of more than 200°. The angle between the magnetic field and the current is varied in steps of 10°, and the recorded resistivity and the corresponding FFT are shown in Fig. 4(a). We observe a shift of dominant α frequency as follows. At $\theta = 0°$ ($B \parallel [001]$), F_α is at 274 T [Fig. 4(b)], and on the gradually tilting the field towards 90° ($B \parallel [100]$), F_α increases. When θ reaches 30°, a new frequency $F_{\alpha'}$ is encountered just above F_α which decreases on increasing the angle further. This $F_{\alpha'}$ does not correspond to the fundamental frequency and is attributed to the neighboring (100) plane because of crystal symmetry. When B is applied perfectly along [100] at $\theta = 90°$, $F_{\alpha'}$ becomes the fundamental frequency corresponding to the (100) plane whereas F_α of the (001) plane disappears completely. This evolution of frequencies is exactly similar to the γ band in the simple cubic SmB$_6$ topological insulator [31]. From the full angular rotation, we tracked F_α and plotted it against θ [Fig. 4(b)] yielding intriguing results. F_α roughly follows the function $F_\alpha/\cos(\theta - n\pi/2)$ (shown by the blue dashed lines) close to the principal crystallographic axes [001], [100], etc., as seen in Fig. 4(c). The similar inverse cosine behavior for F_α has also been observed in LaSb (from the same family of compounds), and the correlation has been argued to arise from the topological two-dimensional (2D) surface states. However, our *ab initio* calculations in LaBi show the presence of highly anisotropic 3D elongated ellipsoidal electron pockets (aspect ratio $= 7.9$). The cross-sectional area of an ellipsoid and hence the corresponding frequency vary with the tilt angle as $A \sim F \sim \pi ab/\sqrt{\sin^2\theta + (\frac{a^2}{b^2})\cos^2\theta}$, where a and b are semimajor and semiminor axes of the ellipsoid, respectively. When $a/b \gg 1$, the above relation reduces approximately to the inverse cosine for small θ values [32]. In LaBi, when the field is tilted further away from these axes, marked deviation from the inverse cosine relation is seen. We have mapped the experimental frequencies on the calculated angular dependence of Fermi-surface cross sections [shown by red crosses in Fig. 4(c)] and observe a striking correlation between F_α and the extremal cross-sectional area of elongated 3D electron pockets. Hence, we consider the
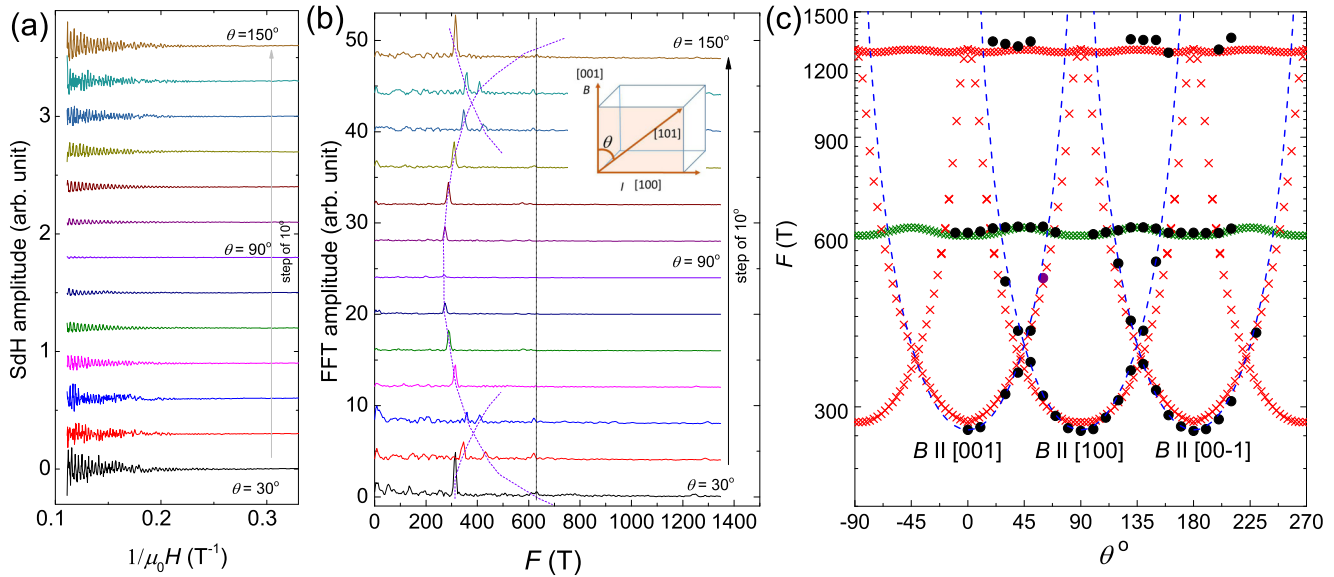
FIG. 4. Angular-dependent SdH oscillations, corresponding FFTs, and fermiology of LaBi. (a) SdH oscillations amplitude [after polynomial (cubic) background subtraction] for tilt angles 30° to 150° (step size 10°). (b) Corresponding FFT amplitudes showing the angular dependence of F_α and F_β. The inset shows the scheme for the field rotation on the (010) plane. (c) Angular dependence of the SdH oscillation frequencies (solid circles) along with the calculated frequencies obtained from the extremal area of 3D Fermi-surface cross sections (the red cross is for the α electron pockets, the green cross is for the β hole pocket) and inverse cosine relation (blue dashed lines). The purple solid circle is the frequency obtained from high magnetic-field measurement up to 35 T.

band corresponding to α to be only pseudo-2D in nature. The frequency corresponding to $\beta(F_\beta)$ is largely independent of the angle. This corresponds very well with the angular-dependent extremal area of an almost spherical hole pocket (β) situated at the Γ point of the Brillouin zone.

To summarize, we show from electrical transport measurements and *ab initio* calculations that, despite having a topologically protected insulating gap, LaBi behaves as a semimetal with very high bulk conductivity. At low temperatures, the anisotropic transport (MR) in lanthanum monopnictides is dominated by highly elongated 3D electron pockets centered

at X points in the Brillouin zone which behave like pseudo-2D and roughly follow the inverse cosine rule. Additionally, the co-presence of highly mobile electron and hole carriers makes LaBi a compensated material with a huge unsaturated MR.

[1] M. Z. Hasan and C. L. Kane, Rev. Mod. Phys. **82**, 3045 (2010).

[2] X.-L. Qi and S.-C. Zhang, Rev. Mod. Phys. **83**, 1057 (2011).

[3] X. Wan, A. M. Turner, A. Vishwanath, and S. Y. Savrasov, Phys. Rev. B **83**, 205101 (2011).

[4] H. Weng, C. Fang, Z. Fang, B. A. Bernevig, and X. Dai, Phys. Rev. X **5**, 011029 (2015).

[5] Z. K. Liu, L. X. Yang, Y. Sun, T. Zhang, H. Peng, H. F. Yang, C. Chen, Y. Zhang, Y. F. Guo, D. Prabhakaran, M. Schmidt, Z. Hussain, S. K. Mo, C. Felser, B. Yan, and Y. L. Chen, Nat. Mater. **15**, 27 (2016).

[6] Z. K. Liu, J. Jiang, B. Zhou, Z. J. Wang, Y. Zhang, H. M. Weng, D. Prabhakaran, S. K. Mo, H. Peng, P. Dudin, T. Kim, M. Hoesch, Z. Fang, X. Dai, Z. X. Shen, D. L. Feng, Z. Hussain, and Y. L. Chen, Nat. Mater. **13**, 677 (2014).

[7] Z. K. Liu, B. Zhou, Y. Zhang, Z. J. Wang, H. M. Weng, D. Prabhakaran, S. K. Mo, Z. X. Shen, Z. Fang, X. Dai, Z. Hussain, and Y. L. Chen, Science **343**, 864 (2014).

[8] C. Shekhar, A. K. Nayak, Y. Sun, M. Schmidt, M. Nicklas, I. Leermakers, U. Zeitler, Y. Skourski, J. Wosnitza, Z. Liu, Y. Chen, W. Schnelle, H. Borrmann, Y. Grin, C. Felser, and B. Yan, Nat. Phys. **11**, 645 (2015).

[9] X. Huang, L. Zhao, Y. Long, P. Wang, D. Chen, Z. Yang, H. Liang, M. Xue, H. Weng, Z. Fang, X. Dai, and G. Chen, Phys. Rev. X **5**, 031023 (2015).

[10] S. Chadov, X. Qi, J. Kübler, G. H. Fecher, C. Felser, and S. C. Zhang, Nat. Mater. **9**, 541 (2010).

[11] H. Lin, L. A. Wray, Y. Xia, S. Xu, S. Jia, R. J. Cava, A. Bansil, and M. Z. Hasan, Nat. Mater. **9**, 546 (2010).

[12] B. Yan and A. de Visser, MRS Bull. **39**, 859 (2014).

[13] C. Shekhar, S. Ouardi, A. K. Nayak, G. H. Fecher, W. Schnelle, and C. Felser, Phys. Rev. B **86**, 155314 (2012).

[14] Z. Hou, W. Wang, G. Xu, X. Zhang, Z. Wei, S. Shen, E. K. Liu, Y. Yao, Y. Chai, Y. Sun, X. Xi, W. Wang, Z. Liu, G. Wu, and X.-X. Zhang, Phys. Rev. B **92**, 235134 (2015).

[15] M. Zeng, C. Fang, G. Chang, Y.-A. Chen, T. Hsieh, A. Bansil, H. Lin, and L. Fu, arXiv:1504.03492.

[16] F. F. Tafti, Q. D. Gibson, S. K. Kushwaha, N. Haldolaarachchige and R. J. Cava, Nat. Phys. **12**, 272 (2016).

[17] J. Nayak, S.-C. Wu, N. Kumar, C. Shekhar, S. Singh, J. Fink, E. E. D. Rienks, G. H. Fecher, S. S. P. Parkin, B. Yan, and C. Felser arXiv:1605.06997.

[18] M. N. Ali, J. Xiong, S. Flynn, J. Tao, Q. D. Gibson, L. M. Schoop, T. Liang, N. Haldolaarachchige, M. Hirschberger, N. P. Ong, and R. J. Cava, Nature **514**, 205 (2014).

[19] K. Wang, D. Graf, L. Li, L. Wang, and C. Petrovic, Sci. Rep. **4**, 7328 (2014).

[20] G. Kresse and J. Hafner, Phys. Rev. B **48**, 13115 (1993).

[21] G. Kresse and J. Furthmüller, Comput. Mater. Sci. **6**, 15 (1996).

[22] J. Heyd, G. E. Scuseria, and M. Ernzerhof, J. Chem. Phys. **118**, 8207 (2003).

[23] N. Marzari and D. Vanderbilt, Phys. Rev. B **56**, 12847 (1997).

[24] I. Souza, N. Marzari, and D. Vanderbilt, Phys. Rev. B **65**, 035109 (2001).

[25] A. A. Mostofi, J. R. Yates, Y.-S. Lee, I. Souza, D. Vanderbilt, and N. Marzari, Comput. Phys. Commun. **178**, 685 (2008).

[26] See Supplemental Material at http://link.aps.org/supplemental/10.1103/PhysRevB.93.241106 for analysis of temperature, magnetic field and angle dependent resistivity for fields up to 9 T and 35 T as well as the description of two band model.

[27] D. V. Khveshchenko, Phys. Rev. Lett. **87**, 206401 (2001).

[28] X. Du, S.-W. Tsai, D. L. Maslov, and A. F. Hebard, Phys. Rev. Lett. **94**, 166601 (2005).

[29] Y. L. Wang, L. R. Thoutam, Z. L. Xiao, J. Hu, S. Das, Z. Q. Mao, J. Wei, R. Divan, A. Luican-Mayer, G. W. Crabtree, and W. K. Kwok, Phys. Rev. B **92**, 180402 (2015).

[30] A. Hasegawa, J. Phys. Soc. Jpn. **54**, 677 (1985).

[31] G. Li, Z. Xiang, F. Yu, T. Asaba, B. Lawson, P. Cai, C. Tinsman, A. Berkley, S. Wolgast, Y. S. Eo, D.-J. Kim, C. Kurdak, J. W. Allen, K. Sun, X. H. Chen, Y. Y. Wang, Z. Fisk, and L. Li, Science **346**, 1208 (2014).

[32] J. M. Schneider, B. A. Piot, I. Sheikin, and D. K. Maude, Phys. Rev. Lett. **108**, 117401 (2012).